

Supplementary Material

Identification of promising compounds from Curry tree with cyclooxygenase inhibitory potential using a combination of machine learning, molecular docking, dynamics simulations and binding free energy calculations

Pujan N. Pandya¹, Sivakumar Prasanth Kumar², Kinjal Bhadresha², Chirag N. Patel¹, Saumya K. Patel¹, Rakesh M. Rawal² and Archana U. Mankad^{1*}

¹Department of Botany, Bioinformatics, and Climate Change Impacts Management, University School of Sciences, Gujarat University, Ahmedabad, India – 380009.

²Department of Life Sciences, University School of Sciences, Gujarat University, Ahmedabad, India – 380009.

Table S1. RF classifier computed using mean impurity decrease method and biochemical roles collected from literature.

S.No	Amino acid	Remarks	Reference	Attribute importance of RF model
1.	Ile344	Literature evidence not available.		5.62
2.	Tyr354	Important active site residue of Human COX-1.	R1, R2	2.7
3.	Ser529	Crucial residue in catalytic pocket. Important residue of COX-1 for aspirin acetylation.	R2, R3	2.68
4.	Arg119	Important residue that constitutes the active site of human COX-1. It helps in forming a h-bond or salt-bridge between COX-1 and arachidonic acid. Severity of aspirin side effects on Arg119Ala & Arg119Gln mutants well demonstrated.	R1, R4	1.99
5.	Leu383	Interacting amino acid residue of COX-1 with ligand (3R)-3-carbamoyl-5-[(1Z)-1-{4-[(4-carboxy-3-hydroxyphenyl) carbamoyl] phenyl} prop-1-en-1-yl]-3H-1,2,4-triazol-1-ium and amarogentin (van der waals interaction).	R1, R5	1.7
6.	Leu533	Important residue of COX-1 in hydrophobic pocket. Daturaolone forms hydrophobic contact with Leu533 of COX-1.	R6	1.67
7.	Met521	Important residue of COX-1 that forms H-bond with ligand eriodictyol (flavanol). Severe effect of aspirin on the COX/POX ratios of mutants Met521Ala and Met521Leu as known.	R7, R8	1.55
8.	Phe380	Interacting amino acid residue (hydrophobic) of COX-1 with ligand 5,5-dihydrogenio-3-[(1Z)-1-[4-({3-hydroxy-4-[hydroxy(λ^3 -oxidanidylidene)methyl]phenyl} carbamoyl)phenyl] prop-1-en-1-yl]-1H-1,2,4-triazol-2-ium and (3R)-3-carbamoyl-5-[(1Z)-1-{4-[(4-carboxy-3-hydroxyphenyl)carbamoyl]phenyl} prop-1-en-1-yl]-3H-1,2,4-triazol-1-ium, chalcone, tetraacetatequercetin.	R1, R9	1.54

9.	Leu352	Important active site residue of Human COX-2.	R10, R11	9.92
10.	Tyr385	Necessary for binding of diclofenac with COX-2. The mutant Tyr385Phe was found to be catalytically inactive compared to its wild type and did not oxidize arachidonic acid when treated with peroxide	R12, R13, R14, R15	4.58
11.	Val344	Crucial active site residue of COX-2.	R10	2.68
12.	Phe518	Important residue positioned at the side pocket for inhibition of COX-2 by meloxicam	R16	2.47
13.	Tyr348	The important residue in hydrophobic pocket critical for NSAIDs interaction with COX-2. The Peroxidase activity of site-directed mutant Tyr348Phe was found to be similar to that of its wild type.	R17, R18, R19	2.07
14.	Tyr355	Crucial active site residues of COX-2 wherein, iodosuprofen and other inhibitors binds. Reduced inhibition of COX-2 mutant Tyr355Phe due to the effect of ligands indomethacin and meclofenamic acid.	R10, R19, R20	2.01
15.	Phe381	Important residue in hydrophobic pocket for binding of NSAIDs with COX-2.	R21	1.73
16.	Phe518	Important residue positioned at the side pocket for inhibition of COX-2 by meloxicam.	R16	1.72

Table S2. Prediction of COX isoform classification using RF model and PLANTS score of MK phytochemicals obeying Lipinski's rule of five.

S. No	MK phytochemicals	Classifier prediction		PLANTS score	
		COX-1	COX-2	COX-1	COX-2
1	2-Napthalenemethanol	0.86	0.97	-58.624	-71.842
2	3-Carene	0.77	0.85	-55.462	-58.634
3	3-Methyl carbazole	0.73	0.9	-62.897	-74.684
4	α -pinene	0.74	0.85	-51.176	-56.534
5	α -Terpinene	0.79	1	-58.631	-63.934
6	β -costol	0.83	0.96	-51.007	-68.808
7	β -elemene	0.87	0.86	-50.320	-60.772
8	β -Eudesmol	0.73	0.88	-54.957	-76.518
9	β -myrcene	0.8	0.86	-58.937	-65.877
10	β -Phellandrene	0.78	0.86	-56.031	-62.170
11	β -pinene	0.72	0.85	-51.743	-58.064
12	β -terpineol	0.71	0.88	-55.556	-63.953
13	Bismurrayaquinone-A	0.77	0.78	43.974	-18.542
14	Borneol	0.73	0.88	-46.243	-53.306
15	Butanedioic acid	0.71	0.86	-52.310	-51.667
16	Camphene	0.7	0.86	-51.193	-55.523
17	Carvomenthone	0.71	0.99	-59.347	-65.205
18	Chrysanthenyl acetate	0.71	0.89	-48.580	-54.566
19	Citral	0.77	0.83	-64.764	-67.788
20	Cubenol	0.73	0.86	-43.864	-71.136
21	Cycloheptane	0.78	0.88	-52.523	-56.134
22	Dipentene	0.78	0.88	-56.975	-61.551
23	Euchrestine-B	0.92	0.95	-65.027	-78.866
24	Eustifoline-D	0.76	0.95	-61.078	-80.342
25	Formylcarbozole	0.72	0.88	-63.540	-79.078
26	Girinimbilol	0.98	1	-62.028	-83.981
27	Girinimbine	0.91	0.88	-46.541	-76.834
28	Glycozoline	0.78	0.94	-63.107	-76.901
29	Heraclenin	1	0.89	-56.090	-71.004
30	Imperatorin	1	1	-58.732	-74.517
31	Dehydroindicolactone	0.9	0.87	-59.453	-69.150
32	Isogirinimbine	0.83	1	-62.685	-82.187
33	Isomahanine	0.83	1	-62.186	-66.320
34	Isomenthone	0.77	1	-54.368	-65.023
35	Juniper camphor	0.8	0.93	-49.730	-67.992
36	Koenigicine	0.78	1	-45.946	-64.970
37	Koenigine	0.83	1	-44.038	-70.312
38	Koeniginequinone-A	0.78	0.92	-55.730	-75.564

39	Koeniginequinone-B	0.82	0.88	-57.195	-77.956
40	Koenimbidine	0.79	0.96	-44.245	-61.408
41	Koenimbine	0.84	1	-47.604	-78.925
42	Koenine	0.87	1	-60.933	-78.707
43	Koenoline	0.83	0.86	-61.464	-81.943
44	Kurryam	0.88	1	-39.901	-70.927
45	Lavandulyl acetate	0.8	0.92	-62.319	-74.370
46	Limonene	0.78	0.88	-56.968	-61.547
47	Linalool	0.75	0.85	-56.689	-63.364
48	Linalyl acetate	0.79	0.84	-65.255	-69.648
49	Mahanine	0.82	0.8	-49.253	-77.981
50	Marmesin-1'- <i>O</i> - β - <i>D</i> -galactopyranoside	0.86	0.92	-30.913	-46.716
51	Menthol	0.72	0.88	-54.433	-62.297
52	Meranzin_hydrate	0.89	0.87	-52.701	-74.063
53	Mukoeic acid	0.8	0.78	-60.771	-80.038
54	Mukoenine-A	0.93	1	-63.231	-84.727
55	Mukoenine-C	0.82	0.9	-56.140	-79.974
56	Mukolidine	0.82	0.94	-60.233	-78.026
57	Mukoline	0.85	0.88	-66.065	-73.531
58	Mukonal	0.72	0.88	-64.795	-79.090
59	Mukonicine	0.8	0.92	-44.628	-72.099
60	Mukonidine	0.77	0.81	-63.900	-81.459
61	Mukonine	0.81	0.8	-64.575	-84.715
62	Murrastanine-A	0.74	0.9	-59.233	-78.647
63	Murrastanine-B	0.85	0.96	-64.831	-88.329
64	Murrastanine-C	0.81	1	-48.521	-79.114
65	Murrayacine	0.84	0.97	-62.026	-71.835
66	Murrayafoline-A	0.82	0.91	-58.448	-74.622
67	Murrayakoeninol	0.79	0.98	-33.839	-52.541
68	Murrayakonine-D	0.91	0.88	-57.084	-58.058
69	Murrayanine	0.82	0.81	-60.788	-81.460
70	Murrayazolinine	0.75	0.89	-31.450	-62.877
71	Murrayazolinol	0.84	0.81	-24.854	-55.524
72	Murrayone	0.88	0.81	-54.165	-72.741
73	Nicotinic acid	0.81	0.8	-53.689	-60.467
74	<i>O</i> -methyl murrayanine	0.8	1	-53.357	-79.876
75	<i>O</i> -methyl murrayamine-A	0.81	1	-56.300	-80.806
76	Sabinene	0.79	0.88	-58.162	-62.605

Table S3. Tanimoto coefficient of MK phytochemicals computed using maximal common substructure search.

MK phytochemicals	Girinimbine	Murrayanine	Murrastinine-B	Mukolidine
Girinimbine	1.00	0.61	0.95	0.61
Murrayanine		1.00	0.58	0.79
Murrastinine-B			1.00	0.58
Mukolidine				1.00

Table S4. Shape similarity analysis of four MK phytochemicals with 21 approved COX-1 inhibitors and 22 approved COX-2 inhibitors.

S. No.	MK phytochemicals	COX-1			COX-2		
		Average	Median	Standard deviation	Average	Median	Standard deviation
1	Girinimbine	0.736	0.744	0.074	0.682	0.709	0.13
2	Murrayanine	0.690	0.691	0.071	0.653	0.674	0.121
3	Murrastinine-B	0.730	0.729	0.067	0.687	0.698	0.126
4	Mukolidine	0.707	0.714	0.076	0.659	0.673	0.126

Table S5. The energetics and structural parameters of the four MK phytochemicals-COX-1 systems from dynamics simulations of 30 ns.

S. No	MK phytochemicals	Total energy of the system (kJ/mol)		
		Minimum	Maximum	Average
1	Girinimbine	-1507158	-1146827	-1150792
2	Murrayanine	-1506345	-1146516	-1150596
3	Murrastinine-B	-1511114	-1147222	-1150573
4.	Mukolidine	-1509171	-1147607	-1151514
S. No	MK phytochemicals	RMSD of the phytochemical (Å)		
		Minimum	Maximum	Average
1	Girinimbine	0.21	1.34	1.02
2	Murrayanine	0.13	1.10	0.54
3	Murrastinine-B	0.13	1.46	0.84
4.	Mukolidine	0.15	1.15	0.96
S. No	MK phytochemicals	R _g of the complex (Å)		
		Minimum	Maximum	Average
1	Girinimbine	23.99	24.63	24.43
2	Murrayanine	24.01	24.86	24.57
3	Murrastinine-B	23.97	24.74	24.49
4.	Mukolidine	23.97	26.64	24.41

Table S6. The energetics and structural parameters of the four MK phytochemicals-COX-1 systems from dynamics simulations of 30 ns.

S. No	MK phytochemicals	Total energy of the system (kJ/mol)		
		Minimum	Maximum	Average
1	Girinimbine	-1582665	-1200214	-1203970
2	Murrayanine	-1582989	-1201420	-1205651
3	Murrastinine-B	-382241	-290680	-291657
4.	Mukolidine	-378824	-287382	-288265
S. No	MK phytochemicals	RMSD of the phytochemical (Å)		
		Minimum	Maximum	Average
1	Girinimbine	0.20	1.37	1.05
2	Murrayanine	0.14	0.91	0.50
3	Murrastinine-B	0.10	1.41	0.79
4.	Mukolidine	0.09	0.89	0.72
S. No	MK phytochemicals	R _g of the complex (Å)		
		Minimum	Maximum	Average
1	Girinimbine	23.91	26.29	25.15
2	Murrayanine	23.92	24.62	24.38
3	Murrastinine-B	23.94	24.75	24.43
4.	Mukolidine	23.92	24.84	24.47

```

      1      10      20      30      40      50      60
F1  FVNPCCIFPCQRQCICVRFCLDRYQCDCGTATCTISCPNCTIPGHWLWLRNSLRPFSFPIHF
F2  FVNPCCIFPCQRQCICVRFCLDRYQCDCGTATCTISCPNCTIPGHWLWLRNSLRPFSFPIHF
consensus>50 FVNPCCYIFPCQRQCICVRFGLDRYQCDCGTATCTISCPNCTIPGHWLWLRNSLRPFSFPIHF

      70      80      90     100     110     120
F1  LLTSCRW#FVFNATFIR#MLMRLVLTVRSNLI#SPPTYN#AHDYISWESFSNVSYTTRI
F2  LLTSCRW#FVFNATFIR#MLMRLVLTVRSNLI#SPPTYN#AHDYISWESFSNVSYTTRI
consensus>50 LLTSCRW#FVFNATFIR#MLMRLVLTVRSNLI#SPPTYN#AHDYISWESFSNVSYTTRI

     130     140     150     160     170     180
F1  LPSVFDCCPTFMCTGKIKQIPDA#ILARRFLRRFIPDPQCTNLMAFFAQHFTHQFFK
F2  LPSVFDCCPTFMCTGKIKQIPDA#ILARRFLRRFIPDPQCTNLMAFFAQHFTHQFFK
consensus>50 LPSVFDCCPTFMCTGKIKQIPDA#ILARRFLRRFIPDPQCTNLMAFFAQHFTHQFFK

     190     200     210     220     230     240
F1  TSCKMCPFTALCHGVDLGHIYCDNLERQYQLRFLKCKLKYQVLF#CEVYPPSVREAPV
F2  TSCKMCPFTALCHGVDLGHIYCDNLERQYQLRFLKCKLKYQVLF#CEVYPPSVREAPV
consensus>50 TSCKMCPFTALCHGVDLGHIYCDNLERQYQLRFLKCKLKYQVLF#CEVYPPSVREAPV

     250     260     270     280     290     300
F1  LMEYFRGIFPFSQ#AVCCQEVVFCLLPCLMLYAT#WLRRENRVCDLLKAEHFTWCDEQLFQT
F2  LMEYFRGIFPFSQ#AVCCQEVVFCLLPCLMLYAT#WLRRENRVCDLLKAEHFTWCDEQLFQT
consensus>50 LMEYFRGIFPFSQ#AVCCQEVVFCLLPCLMLYAT#WLRRENRVCDLLKAEHFTWCDEQLFQT

     310     320     330     340     350     360
F1  ARLLILICETIKIVIEEYVQQLSCTFLQLEKDFPELLFC#QFYRNRRIAMEFNQLYHWHFPLM
F2  ARLLILICETIKIVIEEYVQQLSCTFLQLEKDFPELLFC#QFYRNRRIAMEFNQLYHWHFPLM
consensus>50 ARLLILICETIKIVIEEYVQQLSCTFLQLEKDFPELLFC#QFYRNRRIAMEFNQLYHWHFPLM

     370     380     390     400     410     420
F1  FDSFVYCG#QTSYEQLFNTSMLVDYCV#EALVDAFSRQ#IACRICCCRN#DRIHILVAVDV
F2  FDSFVYCG#QTSYEQLFNTSMLVDYCV#EALVDAFSRQ#IACRICCCRN#DRIHILVAVDV
consensus>50 FDSFVYCG#QTSYEQLFNTSMLVDYCV#EALVDAFSRQ#IACRICCCRN#DRIHILVAVDV

     430     440     450     460     470     480
F1  IKESR#R#RLQFFNEYRKRRCMKFYTSFQEL#CEKEMAAELEEYCDIDALEFVPCLLLEK
F2  IKESR#R#RLQFFNEYRKRRCMKFYTSFQEL#CEKEMAAELEEYCDIDALEFVPCLLLEK
consensus>50 IKESR#R#RLQFFNEYRKRRCMKFYTSFQEL#CEKEMAAELEEYCDIDALEFVPCLLLEK

     490     500     510     520     530     540
F1  CPN#IFCESMIE#CAPFSLKCLLGNP#ICSPFYWR#STFGCEVCF#VKTATLKKLVCLM
F2  CPN#IFCESMIE#CAPFSLKCLLGNP#ICSPFYWR#STFGCEVCF#VKTATLKKLVCLM
consensus>50 CPN#IFCESMIE#CAPFSLKCLLGNP#ICSPFYWR#STFGCEVCF#VKTATLKKLVCLM

     550
F1  I#KCPYVS#VFD
F2  I#KCPYVS#VFD
consensus>50 I#KCPYVS#VFD

```

Figure S1. Sequence alignment of Human COX-1 primary sequence (P1) with PDB template, *Ovis aries* COX-1 sequence (P2). Similar residues are highlighted in red boxes.

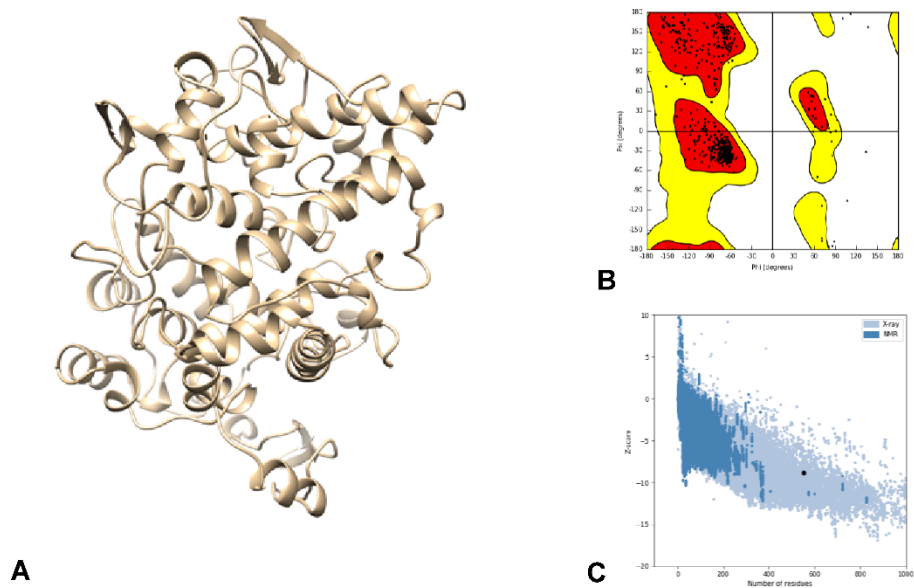


Figure S2. (A) Homology model of Human COX-1 protein structure using the PDB template (PDB ID: 2AYL). (B) Ramachandran plot of the COX-1 model and (C) Data point of COX-1 model in the z -score ProSA map.

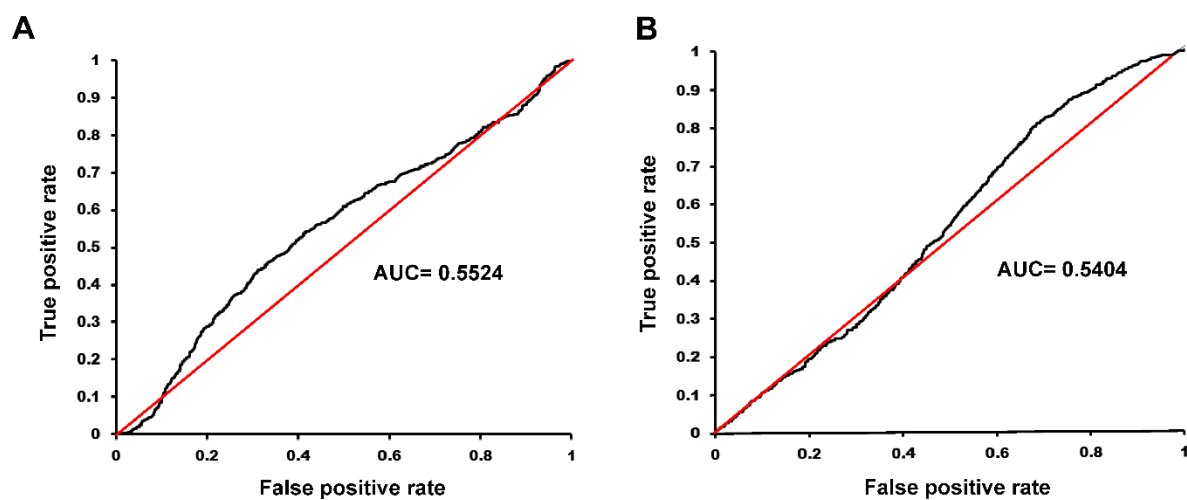


Figure S3. ROC-AUC analysis of PLANTS score obtained from docking exercise of (A) COX-1 and (B) COX-2 actives and decoys.

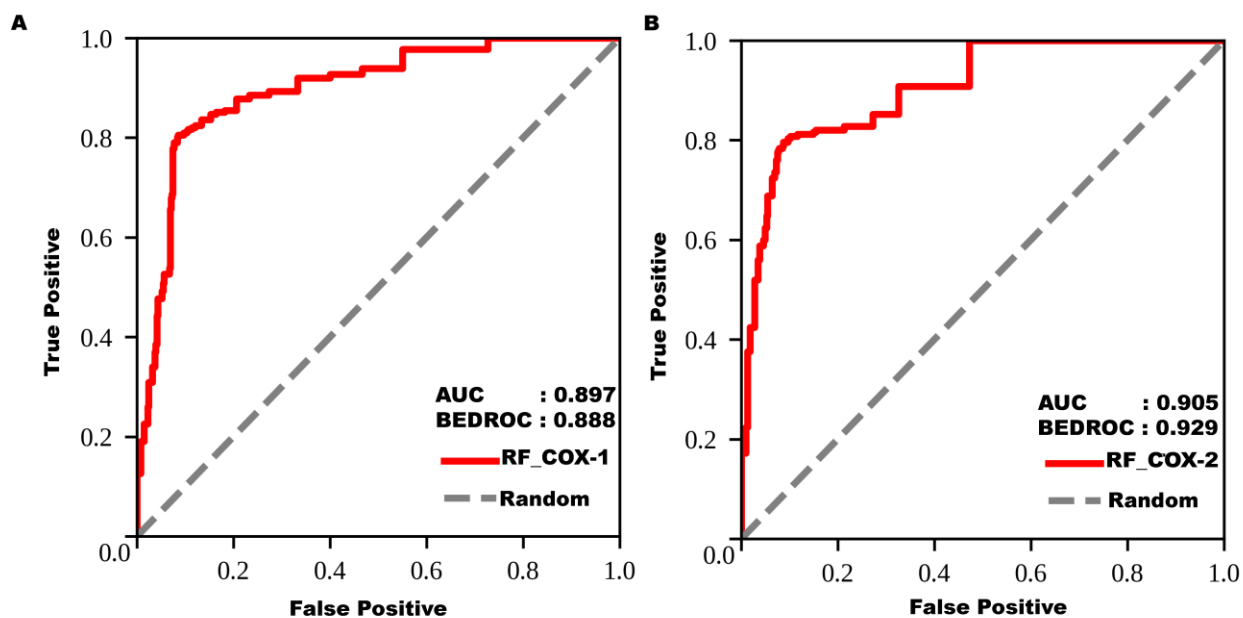
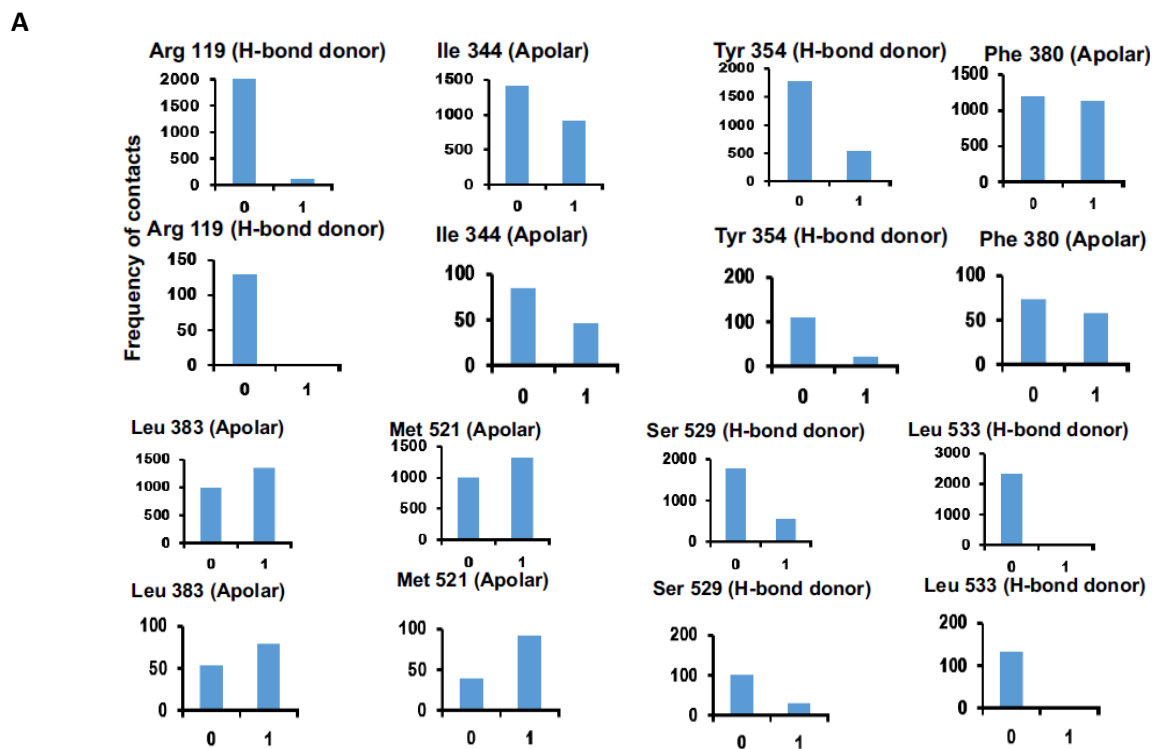


Figure S4. BEDROC analysis of COX isoform specific RF classifiers trained on structural interaction fingerprints. (A) COX-1 specific RF classifier (B) COX-2 specific RF classifier



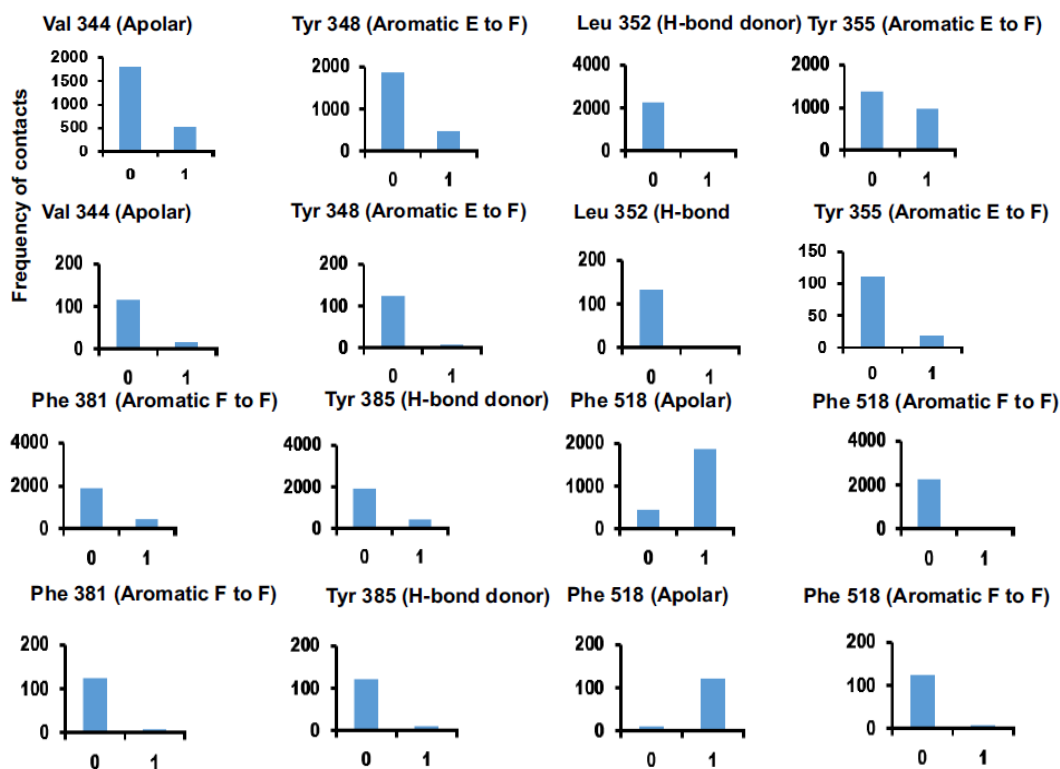
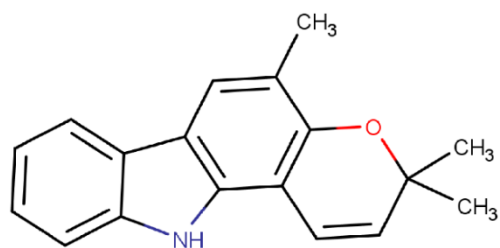
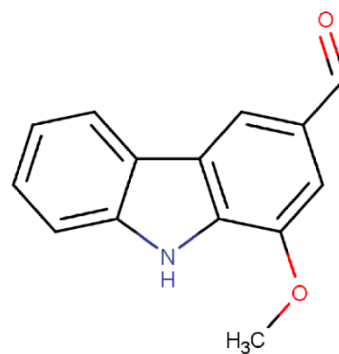
B

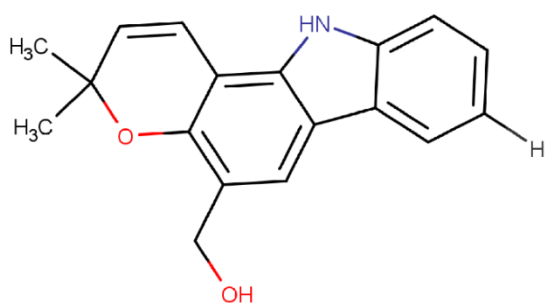
Figure S5. Applicability domain of top 8 interactions of (A) COX-1 and (B) COX-2 targets. In each set, the first and third rows indicate the absence (0) and presence (1) of the interaction types derived from training set whereas the second and fourth rows illustrate the mapping of the respective interaction types in the dock poses of MK phytochemical collection.



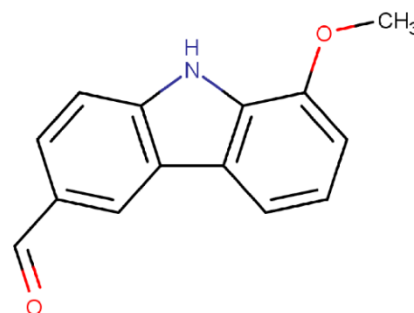
Girinimbine



Murrayanine



Murrastinine-B



Mukolidine

Figure S6. 2D structure of the selected four MK phytochemicals explored in this study.

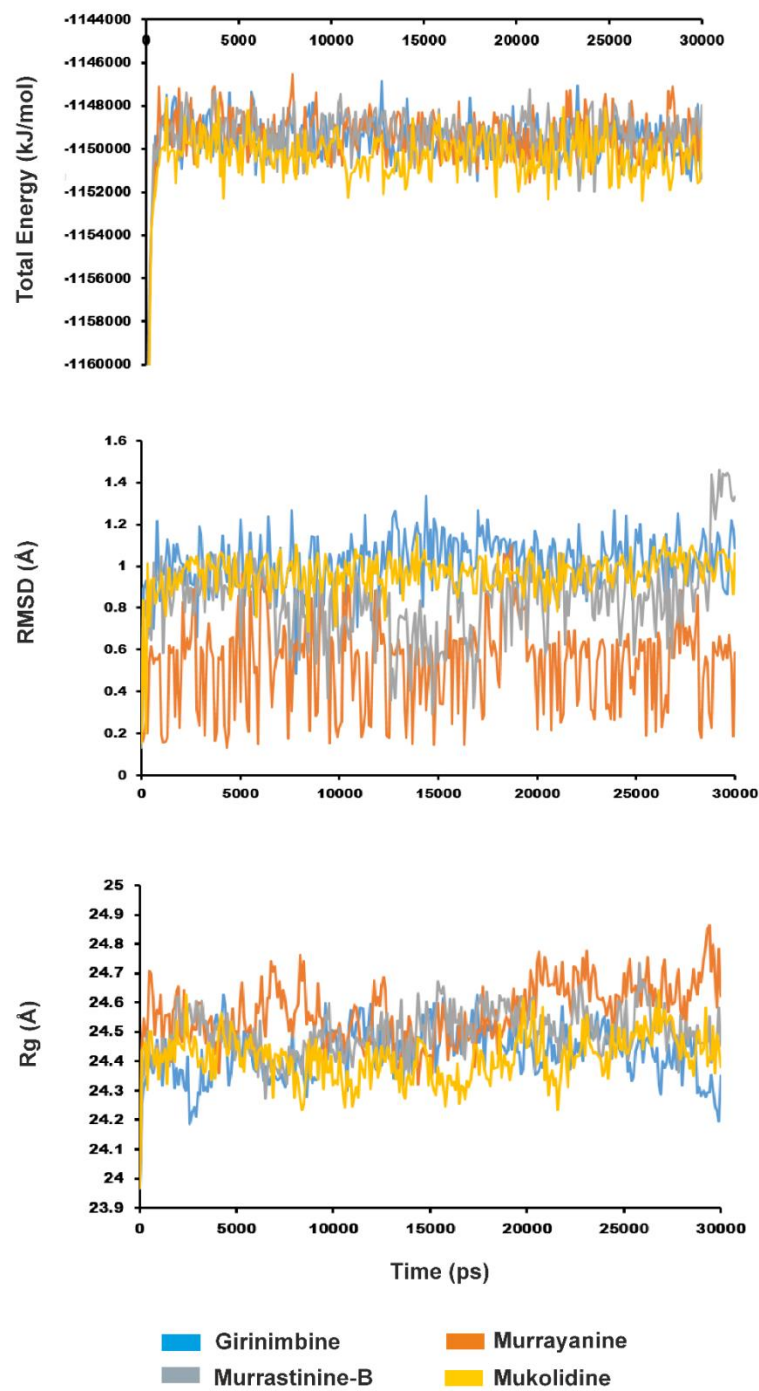


Figure S7. Various evaluation measures of the dynamics simulation of four MK phytochemicals with COX-1 enzyme.

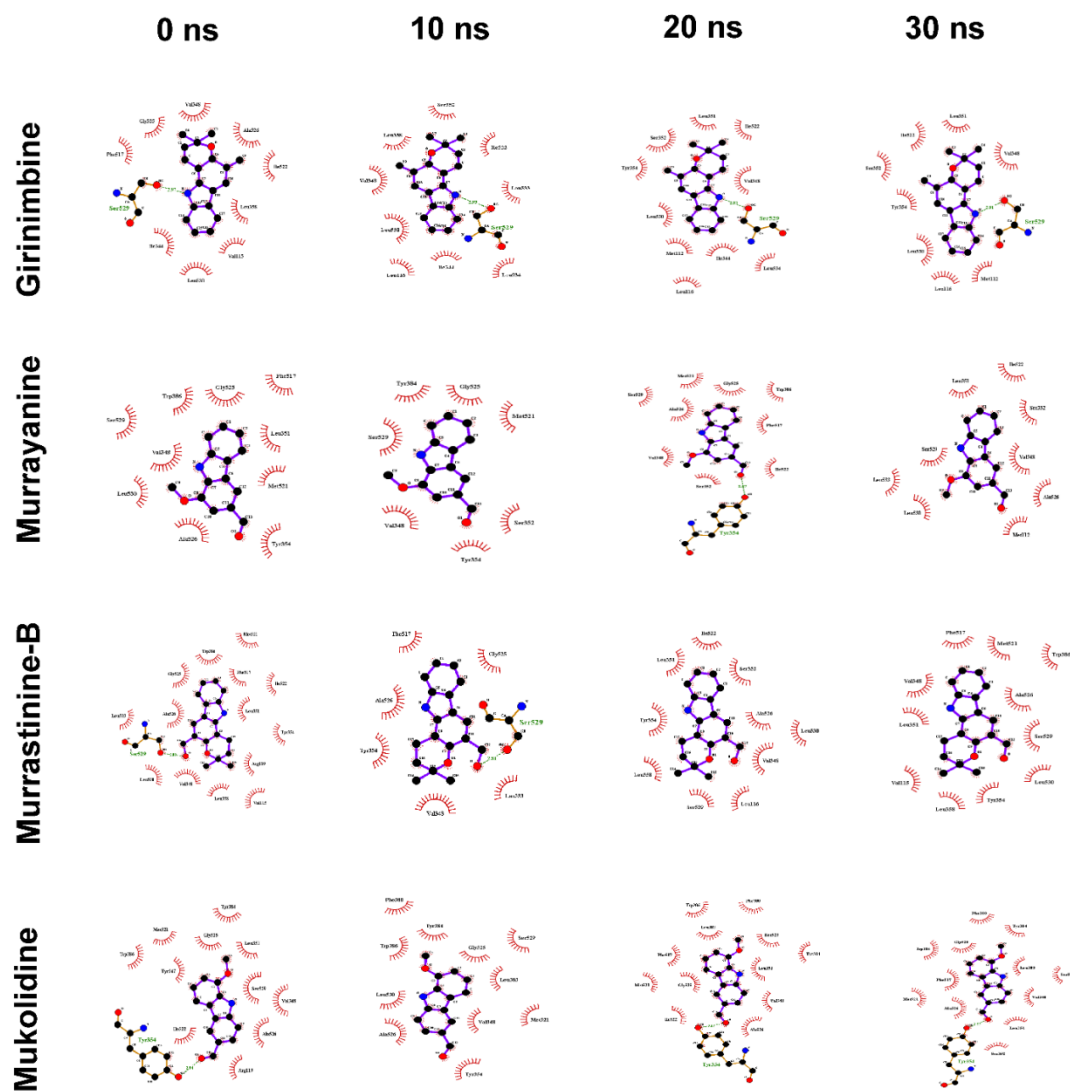


Figure S8. The top four MK phytochemicals interactions with COX-1 enzyme plotted using LigPlot+ program at regular intervals of the simulations trajectory of 30 ns.

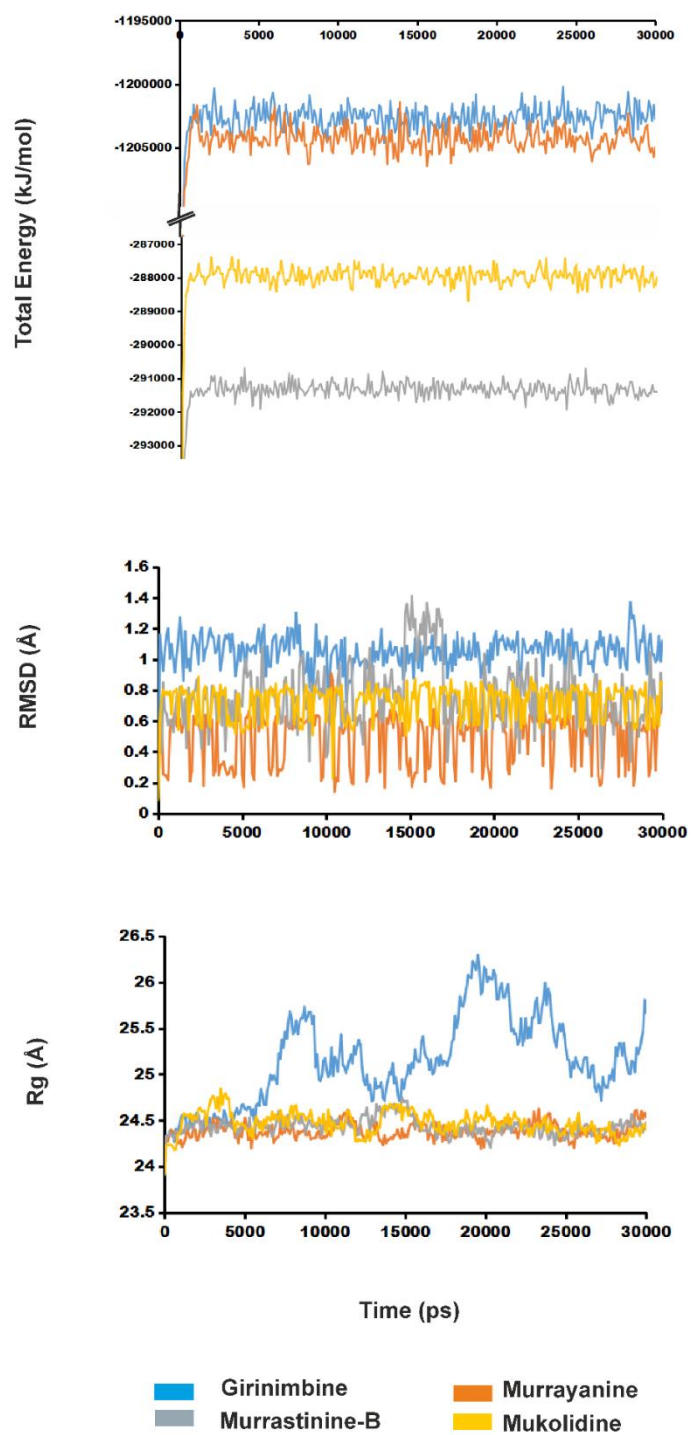


Figure S9. Various evaluation measures of the dynamics simulation of four MK phytochemicals with COX-2 enzyme.

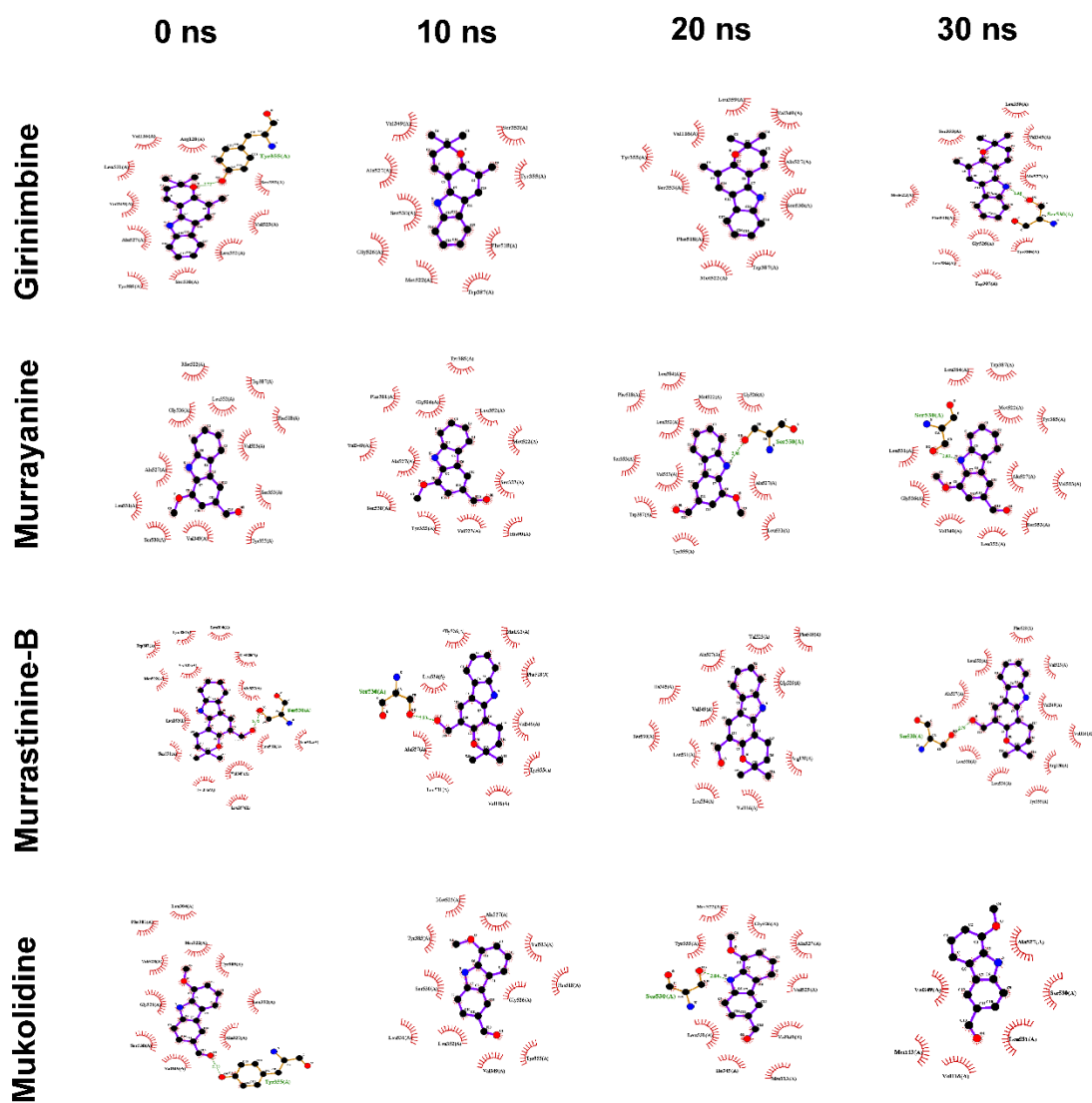


Figure S10. The top four MK phytochemicals interactions with COX-2 enzyme plotted using LigPlot+ program at regular intervals of the simulations trajectory of 30 ns.

Cytotoxicity testing of crude extracts of MK plant

Collection of MK plant material and preparation of extracts

The MK plant materials *viz.* root, stem and leaf samples were collected from the Botanical garden of Department of Botany, Bioinformatics and Climate Change Impacts Management, Gujarat University. The collected samples were washed with distilled water and air-dried at room temperature. The dried samples were powdered using mixture grinder and stored in an air-tight container for further use. The hydroalcoholic crude plant extracts for all three samples were prepared by Soxhlet apparatus using the solvent system consisting of 70% methanol and 30% distilled water [R22]. The extracts were collected in the different petri dishes and allowed to dry at the room temperature. A stock extract of 100 mg in 10 ml solvent system was prepared and was further diluted for the assay.

Procurement and culture of MDA-MB-231 cell line

MDA-MB-231 human breast cancer cell line was obtained from NCCS Pune, India. MDA-MB-231 cells were cultured in DMEM supplemented with 10 % (v/v) heat-inactivated FBS, 2 mM L-glutamine, 100 U/ml of penicillin, and 100 µg/ml of streptomycin. Cells were cultured in 75 cm² culture flasks at 37 °C under the humid environment in an incubator having 5% CO₂.

Cytotoxicity assessment using MTT assay

The effect of MK root, stem and leaves extract on cell viability was measured by MTT assay following the Mosmann protocol [R23]. In brief, the cells (1×10^5 cells per ml) were seeded in a 96 well plate (100 µl per well) with replications. Treatment was performed for 24 h with different concentrations of hydroalcoholic extracts of MK plant parts. After incubation, 20 µl of 5 mg/ml MTT stock solution was added to each well and incubated for 4 h at 37 °C. The obtained formazan crystals were solubilized with DMSO and the absorbance was measured at 570 nm using a microplate reader (Epoch). Cell viability (%) has been shown as a ratio of absorbance (A_{570}) in treated cells to absorbance in control cells (0.1 % DMSO) (A_{570}). The IC₅₀ values were calculated as the concentration of the sample needed to reduce 50 % of the absorbance in comparison to the DMSO-treated control. Percent cell viability was calculated following the equation:

$$\text{Cell viability (\%)} = [A_{570}(\text{Sample})/A_{570}(\text{Control DMSO})] \times 100$$

Results

Cytotoxicity and cell viability assessments of MK extracts using MTT assay

The MTT assay of the hydroalcoholic extracts of different MK plant parts *viz.* root, stem and leaves was performed on the breast cancer cell line MDA-MB-231 to study cell viability and cytotoxicity (Figure S11). Five serial dilutions of the hydroalcoholic extracts were made from the stock solution to perform MTT assay. We observed a trend of cytotoxicity: the cytotoxicity (%) decreases with the decreasing concentration of plant extracts of root and stem (Table S7). Moreover, the IC₅₀ values of the MK plant extracts were estimated based on the measure of optical density. The IC₅₀ values of the stem (0.006 µg/ml), root (0.012 µg/ml) and leaves (0.009 µg/ml) extract revealed that the stem extract is more potent than the other two extracts. The phytochemicals present in the stem might be responsible for its inhibitory potential against the Human breast cancer cell line MDA-MB-231.

Table S7. The viability and cytotoxicity of the extracts of different MK plant parts on the breast cancer cell line MDA-MB-231, determined using MTT assay

S. No.	Cell viability (%)			Cytotoxicity (%)		
	Stem	Root	leaves	Stem	Root	leaves
Control	100	100	100	0	0	0
10 µg	35.02	5.14	12.68	64.98	94.86	87.32
1 µg	36.67	34.98	44.68	63.33	65.02	55.32
100 ng	37.14	38.83	36.39	62.86	61.17	63.60
10 ng	49.15	52.81	50.53	50.84	47.19	49.47
1 ng	67.53	60.66	58.81	32.47	39.34	41.19

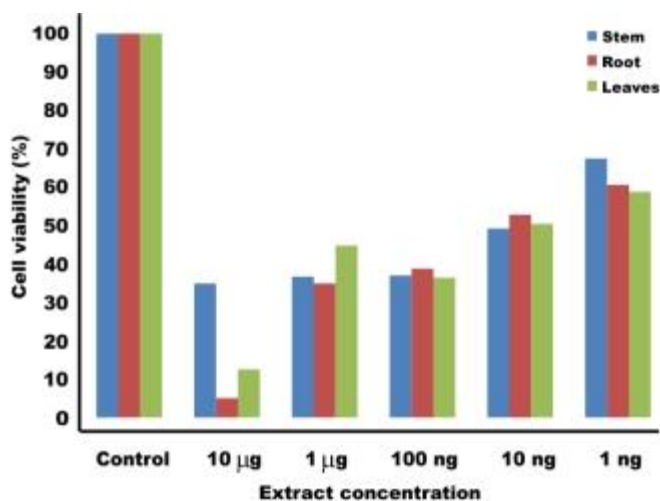


Figure S11. Cell viability as a function of increasing extract concentrations from different MK plant parts estimated by MTT assay on MDA-MB-231 cell line.

The three prioritized MK phytochemicals, girinimbine, murrayanine and murrastinine-B belong to carbazole alkaloid class of phytochemicals. Girinimbine is present in the leaves, stem, roots, fruits and seeds part of MK plant. Murrayanine is present in the stem and leaves parts. Murrastinine-B is present in the bark and leaves parts. Mukolidine, a minor alkaloid is present in the roots and leaves parts. Results of cytotoxicity assay indicates that the IC₅₀ value of stem crude extract proves to be better amongst the other extracts highlighting the important role of phytochemicals present in the stem part.

References

- R1. Dhanjal JK, Sreenidhi, AK, Bafna K, et al. Computational structure-based de novo design of hypothetical inhibitors against the anti-inflammatory target COX-2. *PloS one*, 2015; *10*(8): e0134691, 1-18. <https://doi.org/10.1371/journal.pone.0134691>.
- R2. Chandrasekharan NV. & Simmons D L. The cyclooxygenases. *Genome biology*, 2004; *5*(9), 241,1-7. <https://doi.org/10.1186/gb-2004-5-9-241>.
- R3. Finamore F, Reny JL, Malacarne S, et al. A high glucose level is associated with decreased aspirin-mediated acetylation of platelet cyclooxygenase (COX)-1 at serine 529: A pilot study. *J Proteomics*, 2019; *192*, 258-266. <https://doi.org/10.1016/j.jprot.2018.09.007>.
- R4. Marjan MN, Hamzeh MT, Rahman E, & et al., A computational prospect to aspirin side effects: Aspirin and COX-1 interaction analysis based on non-synonymous SNPs. *J Comp biol Chem*, 2014; *51*, 57-62. <https://doi.org/10.1016/j.compbiolchem.2014.05.002>.
- R5. Shukla S, Bafna K, Sundar D., et al. The bitter barricading of prostaglandin biosynthesis pathway: understanding the molecular mechanism of selective cyclooxygenase-2 inhibition by amarogentin, a secoiridoid glycoside from *Swertia chirayita*. *PloS one*, 2014; *9*(3): e90637,1-16 <https://doi.org/10.1371/journal.pone.0090637>.
- R6. Owoyele BV, Yakubu MT, & Treister R. Pain and Inflammation: Update on Emerging Phytotherapy, Zootherapy, and Nutritional Therapies. *Evid Based Complement Alternat Med*, 2016. <https://doi.org/10.1155/2016/4098686>.
- R7. Akinloye, O A, Metibemu DS, Akinloye D I., et al. Flavanones from *Sorghum bicolor* selectively inhibit COX-2: in-silico and in-vivo validation. *Egypt J of Medl Hum Genet*, 2019; *20*(1), 1-15. <https://doi.org/10.1186/s43042-019-0029-y>.
- R8. Liu W, Poole EM, Ulrich CM, Kulmacz RJ. Decreased cyclooxygenase inhibition by aspirin in polymorphic variants of human prostaglandin H synthase-1. *Pharmacogenet Genomics*. 2012;*22*(7):525–537. <https://doi.org/10.1097/FPC.0b013e32835366f6>.

R9. Shrivash MK, Mishra S, Panwar S L., et al. Attenuation of Pathogenicity in *Candida albicans* by Application of Polyphenols. *J Microb Biochem Technol*, 2018; *10*(2), 27-39. <https://doi.org/10.4172/1948-5948.1000392>

R10. Furse KE, Pratt DA, Porter NA, et al. Molecular dynamics simulations of arachidonic acid complexes with COX-1 and COX-2: insights into equilibrium behavior. *Biochemistry*, 2006; *45*(10), 3189–3205. <https://doi.org/10.1021/bi052337p>

R11. Musfiroh I, Muhtadi A, Kartasmita RE, et al. *In silico* study of asiatic acid interaction with inducible nitric oxide synthase (iNOS) and cyclooxygenase-2 (COX-2). *Int J Pharm PharmSci*, 2013; *5*(Suppl 1), 204-207.

R12. Gierse JK, McDonald JJ, Hauser SD., et al., A single amino acid difference between cyclooxygenase-1 (COX-1) and– 2 (COX-2) reverses the selectivity of COX-2 specific inhibitors. *J Biol Chem*, 1996; *271*(26), 15810-15814. <https://doi.org/10.1074/jbc.271.26.15810>.

R13. Smith WL, DeWitt DL, & Garavito RM. Cyclooxygenases: structural, cellular, and molecular biology. *Annu Rev Biochem*, 2000; *69*(1), 145-182. <https://doi.org/10.1146/annurev.biochem.69.1.145>

R14. Shamsara J, & Shahir-Sadr A, Developing a CoMSIA Model for Inhibition of COX-2 by Resveratrol Derivatives. *Iran J Pharm Res*, 2016;*15*(3), 459–469.

R15. Marnett LJ, Rowlinson SW, Goodwin DC, et al. (1999). Arachidonic acid oxygenation by COX-1 and COX-2 Mechanisms of catalysis and inhibition. *J Biol Chem*, *274*(33), 22903-22906. <https://doi.org/10.1074/jbc.274.33.22903>.

R16. Xu, S., Hermanson, DJ, Banerjee S, Ghebreselasie K, et.al., Oxicams bind in a novel mode to the cyclooxygenase active site via a two-water-mediated H-bonding network. *J Biol Chem*, 2014; *289*(10), 6799-6808. <https://doi.org/10.1074/jbc.M113.517987>.

R17. Vigorita MG, Ottanà R, Monforte F, Maccari, R. et al., Chiral 3, 3'-(1, 2-Ethanediy1)-bis [2-(3, 4-dimethoxyphenyl)-4-thiazolidinones] with anti-inflammatory activity. Part 11: Evaluation of COX-2 selectivity and modelling. *Bioorg Med Chem*, 2003; *11*(6), 999-1006. [https://doi.org/10.1016/S0968-0896\(02\)00518-7](https://doi.org/10.1016/S0968-0896(02)00518-7).

R18. Garavito, R. M., & Mulichak, A. M. (2003). The structure of mammalian cyclooxygenases. *Annu Rev of Bioph Biom*, *32*(1), 183-206. <https://doi.org/10.1146/annurevv.biophys.32.110601.141906>.

R19. Rowlinson SW, Kiefer JR, Prusakiewicz JJ, et al., A novel mechanism of cyclooxygenase-2 inhibition involving interactions with Ser-530 and Tyr-385. *J Biol Chem*, 2003; *278*(46), 45763-45769. <https://doi.org/10.1074/jbc.M305481200>.

R20. Marnett LJ, Rowlinson SW, Goodwin D C., et al., Arachidonic acid oxygenation by COX-1 and COX-2 Mechanisms of catalysis and inhibition. *J Biol Chem*, 1999; 274(33), 22903-22906. <https://doi.org/10.1074/jbc.274.33.22903>

R21. Sakya S M, Hou X, Minich ML, et al., 5-Heteroatom substituted pyrazoles as canine COX-2 inhibitors. Part III: Molecular modeling studies on binding contribution of 1-(5-methylsulfonyl) pyrid-2-yl and 4-nitrile. *Bioorg Med Chem Lett*, 2007; 17(4), 1067-1072. <https://doi.org/10.1016/j.bmcl.2006.11.026>

R22. Pandya PN, Rajhans S, Patel FR, et al. Phytochemical screening of *Murraya koenigii* (L.) Spreng. *Int. J. Res. Adv. Technol.* 2019;7(4),572-576.

R23. Mosmann T. Rapid colorimetric assay for cellular growth and survival: application to proliferation and cytotoxicity assays. *J Immunol Methods*. 1983; 65(1-2), 55-63. [https://doi.org/10.1016/0022-1759\(83\)90303-4](https://doi.org/10.1016/0022-1759(83)90303-4).